Free-boundary plasma equilibria with toroidal plasma flows

W. J. Chen[1], Z. W. Ma[1,a)], H. W. Zhang[1], W. Zhang[1], L. W. Yan[2]

1 Institute for Fusion Theory and Simulation, Zhejiang University, Hangzhou 310027, China

2 Southwestern Institute of Physics, Chengdu, Sichuan 610225, China

a) Corresponding Author E-mail: zwma@zju.edu.cn

abstract

Magnetohydrodynamic equilibrium schemes with toroidal plasma flows and the scrape-off layer are developed for the 'divertor-type' and 'limiter-type' free boundaries in the tokamak cylindrical coordinator. With a toroidal plasma flow, the flux functions are considerably different under the isentropic and isothermal assumptions. The effects of the toroidal flow on the magnetic axis shift are investigated. In a high beta plasma, the magnetic shift due to the toroidal flow are almost the same for both the isentropic and isothermal cases, and are about $0.04a_0$ (a_0 is the minor radius) for M_0=0.2 (the toroidal Alfvèn Mach number on the magnetic axis). In addition, the X-point is slightly shifted upward by 0.0125 a_0. But the magnetic axis and the X-point shift due to the toroidal flow may be neglected because M_0 is usually less than 0.05 in a real tokamak. The effects of the toroidal flow on the plasma parameters are also investigated. The high toroidal flow shifts the plasma outward due to the centrifugal effect. Temperature profiles are noticeable different because the plasma temperature is a flux function in the isothermal case.

I. Introduction

In the past decades, plasma flows have been observed in almost all tokamaks. It can be either spontaneous[1] or driven by neutral beam injection[2] or radio frequency wave heating[3]. Some advance diagnostic technologies have been developed to measure plasma flow, such as charge exchange recombination spectroscopy (CXRS)[4], imaging x-ray crystal spectrometer (XCS)[5], Doppler coherence imaging spectroscopy (Doppler CIS)[6][7] and Langmuir probe. With diagnostic developments, the effect of plasma flows has been investigated intensively. It is found that either toroidal or poloidal plasma flows could suppress macroscopic stabilities , such as (double) tearing mode (TM)[8][9] and resistive wall mode (RWM)[10], and then largely improve both energy and momentum confinement[11][12]. The penetration properties of the n = 1 resonant magnetic perturbation (RMP) is also strongly correlated with toroidal flows[13][14].

For static and ideal plasma, the equilibrium with the axisymmetric assumption can be obtained by solving the well-known Grad-Shafranov (GS) equation that is the nonlinear elliptic partial differential equation for poloidal magnetic flux ψ. There are two free flux functions, pressure $p(\psi)$ and poloidal current function $F(\psi)$, in the GS equation. Several famous static equilibrium codes, such as CHEASE[15], EFIT[16][17], HELENA[18], NOVA q-solver[19] and so on, were developed to solve the GS equation successfully. In order to consider a toroidal plasma flow in the equilibrium, the GS equation has to be generalized. Several codes, such as FLOW[20], ATEC[21], CLIO[22], FINESSE[23], and M3D equilibrium solver[24], have also been developed to solve the generalized Grad-Shafranov (GGS) equation[25][26], which is able to obtain two types of the equilibria: isentropic equilibrium and isothermal equilibrium.. In the isentropic equilibrium, it is assumed that the entropy S=$S(\psi)$ is constant on magnetic surfaces, which considers the isotropic plasma and holds for isentropic flow $\mathbf{B}\cdot\nabla S\left(\psi\right)=0$. In the isothermal equilibrium, the plasma temperature is assumed to a surface quantity T=T(ψ) because of the large heat conductivity along the magnetic field line within a flux surface, which implies isothermal flow $\mathbf{B}\cdot\nabla T(\psi)=0$. In this paper, a detailed comparison between these two equilibria is presented.

The boundary condition at the plasma surface can be chosen to be either a fixed boundary, where plasma-vacuum boundary is replaced by a surface of a perfect conductor[27], or a free boundary as shown in Figure 1. In this paper, we give construction schemes to solve the GGS equation for isentropic and isothermal equilibria with toroidal plasma flows for two different types of the free boundary condition. For the first type of the free boundary problem that is also called the 'limiter-type' free boundary, the plasma equilibrium is solved under an external field by imposing a constraint such as a fixed point where plasma interacts with the limiter. In the second type of the free boundary, namely the 'divertor-type' free boundary, the plasma-vacuum boundary flux value ψ, the position and the shape of plasma are unknown beforehand and defined by a set of external coils and plasma current[24][28].

Three-dimensional toroidal magneto-hydrodynamics code (CLT, Ci-Liu-Ti, which means magnetohydrodynamics in Chinese) has been modified to include a free-boundary equilibrium solver (called CLT-EQ) with toroidal flows and the scrape-off layer (SOL)[8]. A cylindrical coordinator (R, ϕ, Z) is used to avoid the singularity at the central point, r=0, in the toroidal coordinator (ψ, θ, ξ). However, the cylindrical coordinate makes the outer boundary to be more difficult handling because the plasma boundary at the plasma last close surface does not locate at the grid points in the old version of CLT[8]. The current version of the CLT code has been modified with a free plasma boundary and consists of the X point, the separatrix, and the SOL. With a free plasma boundary, CLT has the capability to calculate self-consistently in the plasma edge region.

The rest of this paper is organized as follows: in Section II, isentropic and isothermal equilibrium formulations with a toroidal plasma flow are present. In Section III, a detail construction scheme to solve the GGS equation with a free boundary is discussed. To be more specific, different plasma regions in the computational domain are defined in order to construct the current source. The Green's function method is adopted for external coils. In Section IV, the solving procedure used in CLT-EQ is described. Numerical results of the isentropic and isothermal equilibria for the two different types of the free boundary with toroidal plasma flows are presented in Section V. The conclusion and discussion are given in Section VI.

II. Formulation of Isentropic and Isothermal Equilibria for Toroidal Plasma Flow

We start with the steady-state ideal magnetohydrodynamics (MHD) equations in a cylindrical coordinate (R, ϕ, Z) with $\partial/\partial\phi = 0$. The MHD equations with plasma flows are as follows:

$$\nabla \cdot (\rho \boldsymbol{v}) = 0 \tag{1}$$

$$\rho (\boldsymbol{v} \cdot \nabla) \boldsymbol{v} = \boldsymbol{J} \times \boldsymbol{B} - \nabla p \tag{2}$$

$$\nabla \times \boldsymbol{E} = 0 \tag{3}$$

$$\nabla \cdot \boldsymbol{B} = 0 \tag{4}$$

$$\mu_0 \boldsymbol{J} = \nabla \times \boldsymbol{B} \tag{5}$$

$$\boldsymbol{E} = -\boldsymbol{v} \times \boldsymbol{B} \tag{6}$$

where ρ, p, $\boldsymbol{v}$, J, $\boldsymbol{B}$ and $\boldsymbol{E}$ are the plasma density, the pressure, the plasma flow velocity, the current density, the magnetic field, and the electric field. Let $\psi(R,Z) = \int \mathbf{B} \cdot d\mathbf{s} \big/ 2\pi = \int_0^R R' B_z dR'$ be the poloidal-disk flux[29]. Then, the magnetic field can be expressed as $\mathbf{B} = \nabla\phi \times \nabla\psi + B_\phi \mathbf{e}_\phi$, $B_R = -\dfrac{1}{R}\dfrac{\partial \psi}{\partial Z}$ and $B_Z = \dfrac{1}{R}\dfrac{\partial \psi}{\partial R}$, where B_R and B_Z are the horizontal and vertical magnetic fields. From $\mu_0 \mathbf{J} = \nabla \times \mathbf{B}$, then

$$\Delta^* \psi = -\mu_0 R J_\phi , \tag{7}$$

where J_ϕ is the toroidal plasma current density and $\Delta^* = R^2 \nabla \cdot \left(\nabla / R^2 \right)$. The poloidal flux is able to be determined by Eq. (7), if J_ϕ and the boundary condition are known. In the following, we will discuss the expression of J_ϕ. Faraday's law $\nabla \times (\boldsymbol{B} \times \boldsymbol{v}) = 0$ and $\boldsymbol{B} \cdot (\boldsymbol{B} \times \boldsymbol{v}) = 0$ imply $\boldsymbol{B} \times \boldsymbol{v} = \Omega(\psi) \nabla \psi$, where $\Omega(\psi)$ is an arbitrary function of the poloidal flux. If only a toroidal flow $\boldsymbol{v} = v_\phi \mathbf{e}_\phi$ is considered, then $\boldsymbol{B} \times \boldsymbol{v} = \nabla\phi \times \nabla\psi \times v_\phi \mathbf{e}_\phi = (v_\phi / R) \nabla \psi$. We have

$$v_\phi = R\Omega(\psi) \tag{8}$$

where $\Omega(\psi)$ is the toroidal angular velocity of the flux surface[26]. Similar to the poloidal flux $\psi(R,Z)$, we define a poloidal current function $F(R,Z) = \int \mu_0 \mathbf{J} \cdot d\mathbf{s} \big/ 2\pi = \int_0^R \mu_0 R' J_z dR'$ and then obtain $J_Z = \dfrac{1}{\mu_0 R}\dfrac{\partial F}{\partial R}$. Using

$\nabla\cdot\nabla\times\mathbf{B}=\mu_0\nabla\cdot\boldsymbol{J}=0$, we have $J_R=-\frac{1}{\mu_0 R}\frac{\partial F}{\partial Z}$ and the poloidal current $\mathbf{J}_p=\left(\nabla F\times\mathbf{e}_\phi\right)/\mu_0 R$. From the R component of the Ampere's law Eq. (5), we get $\mu_0 J_R=-\left(\partial F/\partial Z\right)/R=-\partial B_\phi/\partial Z$, which implied

$$F\left(R,Z\right)=RB_\phi \tag{9}$$

Considering $\left(\boldsymbol{v}\cdot\nabla\right)\boldsymbol{v}=-R\Omega^2\left(\psi\right)\mathbf{e}_R$, the ϕ component of the momentum equation reduces to $\left(-\rho\mathbf{v}\cdot\nabla\mathbf{v}-\nabla p+\mathbf{J}\times\mathbf{B}\right)_\phi=\left(\mathbf{J}\times\mathbf{B}\right)_\phi=\left(\nabla\times\mathbf{B}\times\mathbf{B}\right)_\phi=\left(\mathbf{B}/R\right)\nabla\left(RB_\phi\right)=0$, which means that the poloidal current function $F\left(R,Z\right)=RB_\phi=F\left(\psi\right)$ is also an arbitrary function of the poloidal flux. The momentum equation is written in the following form

$$\frac{J_\phi}{R}\nabla\psi=\nabla p-\rho R\Omega^2\nabla R+\frac{FF'}{R^2}\nabla\psi \tag{10}$$

where prime $'$ denotes $\partial/\partial\psi$. From the momentum equation, $\boldsymbol{B}\cdot\nabla p=\boldsymbol{B}\cdot\left(-\rho\boldsymbol{v}\cdot\nabla\boldsymbol{v}+\boldsymbol{J}\times\boldsymbol{B}\right)=\rho R\Omega^2\boldsymbol{B}\cdot\nabla R\neq 0$ implies the plasma pressure is not a flux surface quantity anymore.

The thermodynamic relationship of p, ρ and T in the presence of the plasma rotation are derived in two forms[25][26] [20] [21]. The first form is that the entropy S=$S(\psi)$ is constant on magnetic surfaces, which considers isotropic plasma and holds for the isentropic flow $\mathbf{B}\cdot\nabla S\left(\psi\right)=0$. The other is that the plasma temperature T=T(ψ) is a surface quantity because of the large heat conductivity along the magnetic field line within a flux surface, which implies the isothermal flow $\mathbf{B}\cdot\nabla T(\psi)=0$. In this paper, both of the isentropic and isothermal equilibria are developed.

For the isentropic case $S(\psi)$, the right-hand side of Eq. (10) can be written in the following form[25][21]:

$$\nabla p-\rho R\Omega^2\nabla R+\frac{FF'}{R^2}\nabla\psi=\rho\nabla\theta_S\left(\psi\right)+\left(-TS'+\rho R^2\Omega\Omega'+\frac{FF'}{R^2}\right)\nabla\psi . \tag{11}$$

We find that $\theta_S\left(\psi\right)=-R^2\Omega^2/2+\frac{\gamma}{\gamma+1}S\rho^{\gamma-1}$ is a surface quantity (see Appendix). Since $\nabla\psi$ cannot be identically zero, Eq. (10) reduces to

$$\frac{J_\phi}{R}=\rho\theta_S^{'}-TS'+\rho R^2\Omega\Omega'+\frac{FF'}{R^2} . \tag{12}$$

For the isentropic case, Eq. (7) and (12) are the general equilibrium equation of an axisymmetric plasma with a toroidal rotation in the cylindrical coordinate, where the entropy is assumed to be constant on magnetic surfaces. There are four arbitrary functions $\theta_S\left(\psi\right)$, $S(\psi)$, $\Omega\left(\psi\right)$ and $F(\psi)$ in Eq. (12). If these four functions and the boundary condition are given, the solution of Eq. (7) is solely determined.

(2) For the isothermal case $T(\psi)$, the right-hand side of Eq. (10) can be written in the following form[25]:

$$\nabla p-\rho R\Omega^2\nabla R+\frac{FF'}{R^2}\nabla\psi=\rho\nabla\theta_T\left(\psi\right)+\left(\rho\left(1-\ln\rho\right)T'+\rho R^2\Omega\Omega'+\frac{FF'}{R^2}\right)\nabla\psi . \tag{13}$$

We find that $\theta_T\left(\psi\right)=-R^2\Omega^2/2+T\ln\rho$ is also a surface quantity (see Appendix). Eq. (10) is reduced to

$$\frac{J_\phi}{R}=\rho\theta_T^{'}+\rho\left(1-\ln\rho\right)T'+\rho R^2\Omega\Omega'+\frac{FF'}{R^2} \tag{14}$$

Similarly, for the isothermal case $T(\psi)$, the solution of Eq. (10) is also solely determined if the four arbitrary functions $\theta_T\left(\psi\right)$, $T(\psi)$, $\Omega\left(\psi\right)$ and $F(\psi)$ in Eq. (14)

and the boundary condition are given.

III. The Construction Scheme for the Free Boundary Conditions

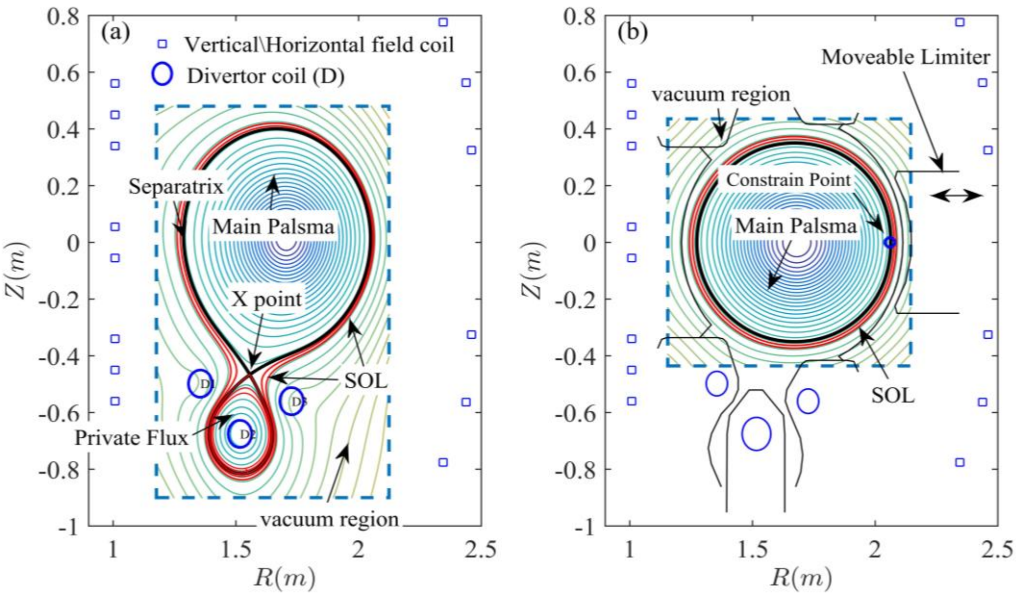

Figure 1. (a) For the 'divertor-type' free boundary in HL-2A tokamak, the computational domain is divided into the main plasma, SOL, the vacuum, the private-flux, and the coil region. Note that the divertor coil is located inside the computational domain. (b) For the 'limiter-type' free boundary, the computation domain is only divided into the main plasma, SOL, and the vacuum region.

In this section, both the 'divertor-type' and 'limiter-type' free boundary are presented. A poloidal cross section of HL-2A tokamak with the divertor and the limiter are shown in Figure (1). Different regions in the computational domain are defined as follow. Firstly, the 'main plasma' region consists $\tilde{\psi}<1$, where $\tilde{\psi}=(\psi-\psi_{axix})/(\psi_b-\psi_{axix})$ is the normalized poloidal flux, ψ_{axix} and ψ_b are the flux at the magnetic axis and the 'main plasma' boundary, respectively. And $\tilde{\psi}=1$ represents the plasma boundary. For the divertor configuration, the boundary is the separatrix or the last closed flux surface (LCFS). For the limiter, the boundary is the isoline of the constraint point where is the interface between the plasma and the limiter. Secondly, the SOL region consists of $1<\tilde{\psi}<\tilde{\psi}_{SOL}$. $\tilde{\psi}_{SOL}-1$ is the width of the SOL region that is roughly interchangeably with the power decay length λ_q that is designed to be about 20 mm ($\tilde{\psi}_{SOL}$~1.03) based on the experiment[30][31]. Thirdly, the vacuum region represents the area where the magnetic field is generated only by non-local currents, such as the plasma current and the external coil. Fourthly, the 'private flux' region (only for the divertor) consists of $\tilde{\psi}<1$ and is located below the X point. SOL is slightly widened into the 'private flux' region. In reality, the plasma region is more complicated than the above definition when the divertor is considered[32].

The main plasma boundary $\tilde{\psi}=1$ is critical for the free boundary plasma equilibrium. For the limiter-type case, the boundary is the isoline of the constraint point where is the interface between the plasma and the limiter. The plasma equilibrium is solved under the external field, as shown in Figure 1(b). It is a bit more complicated for the divertor-type case. In order to produce the real divertor configuration, we need to consider divertor coils as shown in Figure 1(a). Moreover, for the high beta plasma equilibrium, the plasma will shift toward the low field side. Therefore, vertical field coils are designed to generate the vertical magnetic field to push the plasma inward by the Lorentz magnetic force. The shape and the position of the plasma are consistent with these coil currents. According to the position of these external coil, two numerical methods are adopted. If external coils are located inside the computational domain, they are regarded as local plasma currents and the flux ψ can be computed though Eq. (16).

If external coils are located outside the computational domain, the Green's function method will be adopted via Eq. (19).

A. Current Sources Located inside the Computational Domain

Because divertor coils are located inside the computational domain for the 'divertor-type' free boundary, we divide the computation domain into three parts, namely the plasma region (included the main plasma and SOL), the divertor coils region, and the vacuum region (including a part of the private flux area) as shown in Figure 1(a). In the plasma region, the current source is the plasma toroidal current density J_ϕ in Eq. (12) or Eq. (14), so the flux function ψ satisfies Eq. (7). In the vacuum region, there is no current source, so the flux function ψ satisfies

$$\Delta^*\psi = 0 \tag{15}$$

In the divertor coil region, the divertor coil currents are regarded as local plasma currents. Thus, the flux function ψ satisfies

$$\Delta^*\psi = -\mu_0 R J_{Di}\left(R,Z\right) \quad \left(i=1,2,3\right) \tag{16}$$

Three divertor coils, namely D1 (J_{D1}), D2 (J_{D2}), and D3 (J_{D3}), are designed in this scheme. And the coil currents $I_{Di} = \int J_{Di}\left(R,Z\right)ds$, J_{Di} is a parabolic distribution function. The current direction of the D1 and D3 coils must be opposite to that of the plasma current. The current direction the D2 coil is the same as that of the plasma current.

B. Current Sources Located outside the Computational Domain

In this case, because of vertical/horizonal field coils located outside the computational domain as shown in Figure 1, we introduce the Green's function,

$$G(\boldsymbol{x},\boldsymbol{x}')=\frac{\mu_0}{2\pi}\frac{\sqrt{RR'}}{k}\left[\left(2-k^2\right)F(k)-2E(k)\right], \tag{17}$$

where G($\boldsymbol{x}$, $\boldsymbol{x}'$) is the magnetic flux at $\boldsymbol{x}'$=(R',Z') produced by the one Ampere vertical coil current at $\boldsymbol{x}$=(R,Z)[27]. F(k) and E(k) is the first and the second complete elliptic integrals respectively, and $k^2=4RR'\Big/\left[\left(R-R'\right)^2+\left(Z-Z'\right)^2\right]$. This Green's function in Eq. (17) satisfies

$$\Delta^* G(\boldsymbol{x},\boldsymbol{x}')=-\mu_0 R\delta(\boldsymbol{x}-\boldsymbol{x}') \tag{18}$$

Because of the current source located outside the computational domain, this function is reduced as $\Delta^* G(\boldsymbol{x},\boldsymbol{x}')=0$ in the computational domain. Therefore, the total poloidal flux ψ_T is expressed by the Green's function in the following form

$$\psi_T(\boldsymbol{x})=\psi(\boldsymbol{x})+\sum_{i=1}^{N} I_{coil}^{i} G(\boldsymbol{x},\boldsymbol{x}'), \tag{19}$$

where I_{coil}^{i} is the i-th coils current. The Green's function method can be applied to all poloidal field coils that are located outside the computational domain, such as horizontal coils are used to control the plasma vertical displacement while vertical field coils are used to control the plasma horizontal displacement.

IV. Numerical Procedure

Figure 2 is the flowchart of the CLT-EQ code. The equilibrium equation is computed on a 256 × 256 grid of the (R, Z) plane. The solving procedure is as follows.

A. The four parameter functions $\theta_s(\psi)$, $S(\psi)$, $\Omega(\psi)$ and $F(\psi)$ in Eq.(12) or

$\theta_T(\psi)$, $T(\psi), \Omega(\psi)$ and $F(\psi)$ in Eq.(14) are constructed. The profile of the parameter function can be chosen to be surface-averaged data from experiment or be specially designed for simulation requirement. Moreover, the plasma flow Ω is freely adjusted to study effects on the equilibrium by varying the plasma velocity.

B. The initial flux ψ_0 is calculated via a set of external coils and the initial plasma current. ψ_0 is critical for convergence. And it contains information of the plasma shape and displacement.

C. The X point, the separatrix, and the magnetic axis are calculated thought the initial flux ψ_0 or the updated flux ψ. In other word, the position and the flux of the X point are calculated from ψ_0 or ψ, and LCFS is identified through the isoline of the X point. Then the computational domain is divided into the plasma region (including the main plasma and SOL), the vacuum region (including a part of the private flux area), and the divertor coil region. Current sources in each region are obtained via Eq. (12), or (14), (15), (16).

D. Eq. (7, 15, 16) are simultaneously solved using the Strongly Implicit Procedure (SIP) method to update the magnetic flux ψ [28][33][34]. In the nth iteration, the iterative formula is $\Delta^* \psi_{n+1} = -\mu_0 R J_\phi\left(R, \psi_n\right)$. The convergence defined with a condition on the residual of this formula is $\Delta = \sum_{i=1}^{N} \left| \psi_{n+1}^i - \psi_n^i \right| / N \sim 10^{-6}$, where N is the number of grids.

E. Step C and D are iterated until the flux ψ at the end of Step D remains unchanged within a given tolerance.

F. After an equilibrium calculation, we need to check whether plasma is in a reasonable position. If not, external coil currents need to be adjusted in order to obtain a suitable plasma position shown in Figure (3). Meanwhile, the initial poloidal flux ψ_0 is recalculated at Step B. Consequently, the new flux ψ is updated by iteration of Step C, D and E again. In the free-boundary calculation, the boundary condition is imposed during initialization. The X point, the magnetic axis, and the separatrix are not fixed and determined as a part of the solution of the equilibrium problem. Figure 3 is a high beta H-mode equilibrium. In this case, vertical field coil currents produce the vertical magnetic to put the plasma inward by the Lorentz force. Otherwise, the plasma will move to the low field side due to a large thermodynamic force. We note that the boundary is a constraint by a fixed point for the limiter-type case, while the X point is free for the divertor-type case.

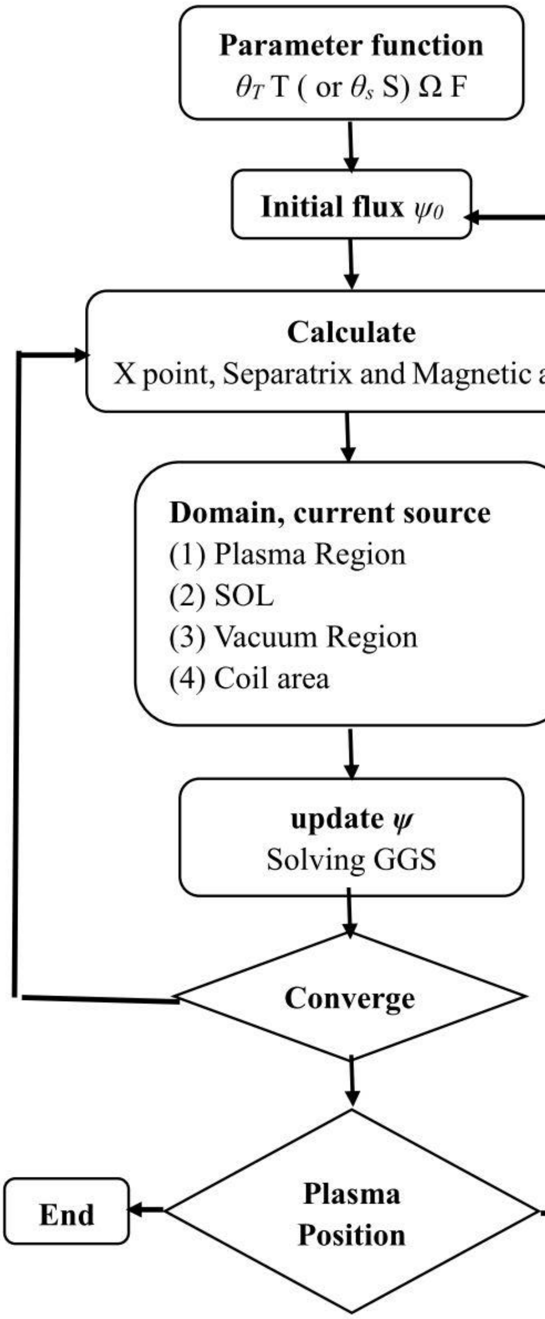

Figure 2. Flowchart of CLT-EQ

258

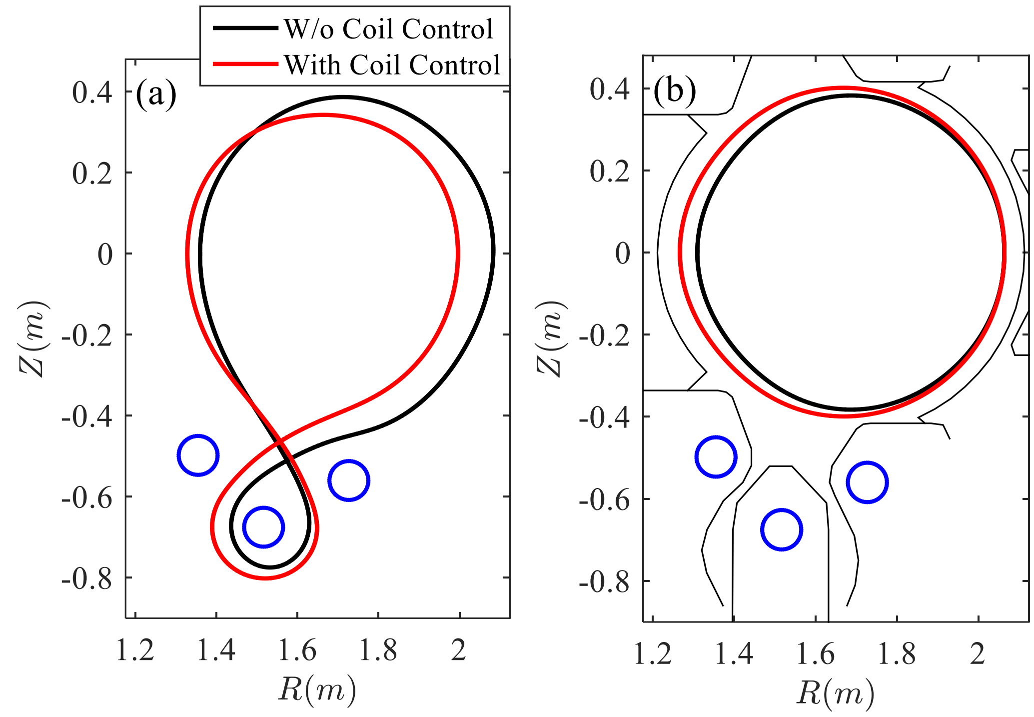

Figure 3. Vertical Coils to control the horizontal displacement

V. Numerical Results

A. Effect of Toroidal Plasma Flow on Magnetic Shift

As we known, the magnetic axis is displaced due to the plasma pressure and the internal inductance, which is named as the Shafranov shift. With the toroidal plasma rotation, the moment equation Eq. (2) can roughly be expressed as $\sim \boldsymbol{J}\times\boldsymbol{B}-\nabla\left[p+\rho\left(v^2/2\right)\right]$, which means that the 'kinetic energy' density, $\rho\left(v^2/2\right)$, like the plasma pressure, also contributes to the Shafranov shift. In order to investigate the effect of the toroidal flow on the magnetic axis shift, we use the toroidal Alfvèn Mach number, $M=v_\phi/v_A$, to quantify the plasma flow. v_A is the Alfvèn speed and M_0 is the toroidal Alfvèn Mach number on the magnetic axis. In order to concentrate on the contribution of the toroidal flow in the Shafranov shift, we subtract the Shafranov shift in the static equilibria $\Delta_{\Omega=0}$ from the total shift Δ_{Ω}, and normalize with the plasma minor radius a_0. The expression $\left(\Delta_{\Omega}-\Delta_{\Omega=0}\right)/a_0$ quantifies the contribution of the toroidal plasma flow to the Shafranov shift as shown in Fig. 4(a) where the red and black lines represent for the isothermal and isentropic cases, respectively. The solid and dashed lines correspond to low beta and high beta plasma, respectively. The magnetic shift is larger at a lower beta plasma or a higher M_0 for both isothermal and isentropic cases, which is not surprising since the "kinetic energy" term, compared with the pressure term in moment equation, will become more important with the plasma beta decrease or the toroidal flow (or M_0) increase. In addition, in the low beta plasma, the magnetic shift in the isothermal case is larger than that in the isentropic case. This difference is more severe when M_0 increases. However, it is seen that the effect of the toroidal rotation on the shift in the high beta plasma is qualitatively similar for both cases. The magnetic shift due to the toroidal flow is about $0.04a_0$ at M_0=0.2. Of more interest is the shift of the X-point due to the toroidal plasma flow as shown in Figure 4(b), which is only calculated in the 'divertor-type' free boundary equilibrium. The X-point is slightly shifted upward by about 0.0125 a_0 for both the isentropic and isothermal cases at M_0=0.2. In reality, M_0 is almost less than 0.05 for most of present tokamaks[11]. Therefore, the effect of the toroidal flow on the magnetic axis and the X-point shift may be neglected.

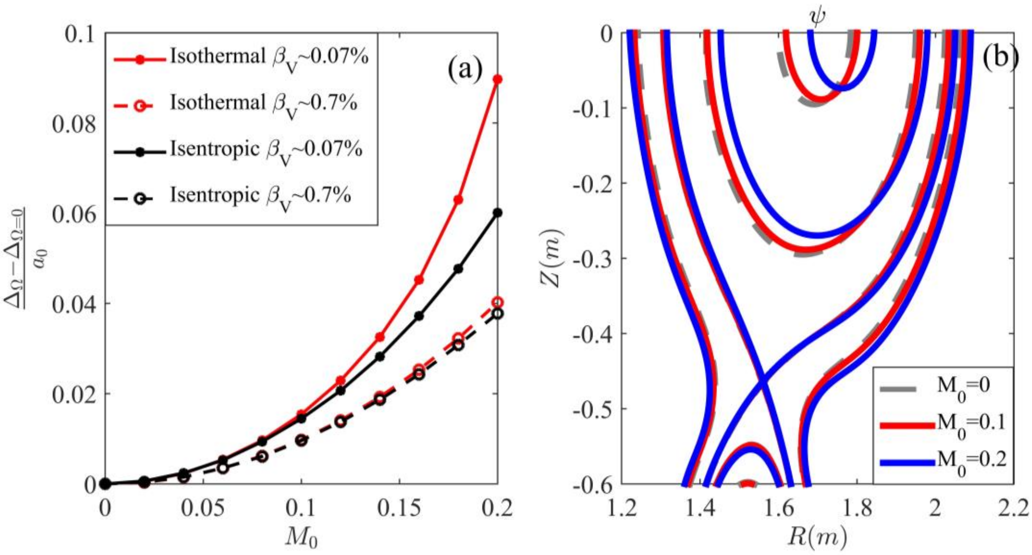

Figure 5 (a) Shafranov shift as function of M_0. Solid and dashed lines correspond to the low and high beta plasma, respectively. Red and black line represent the isothermal and isentropic cases. (b) Magnetic flux surfaces in the presence of the high toroidal flow. The X-point is slightly shifted upward.

B. Effect of Toroidal Flow on Plasma Parameters

The effects of the toroidal flow on Plasma parameters, such as the density, the pressure, and the temperature, are shown in Figure 5 where the red and blue lines represent for the isothermal and isentropic cases, respectively. As we can see that toroidal flow shifts the plasma outward due to the centrifugal effect that is qualitatively similar both in the isothermal and isentropic cases. But there is a noticeable difference in the temperature profile due to the fact that the plasma temperature is a flux function regardless of the flow in the isothermal case. Because the temperature expresses as $T = \rho^{\gamma-1}/(\gamma-1)$ in the isotropic case, the profile shift in the temperature is similar to that in the plasma density.

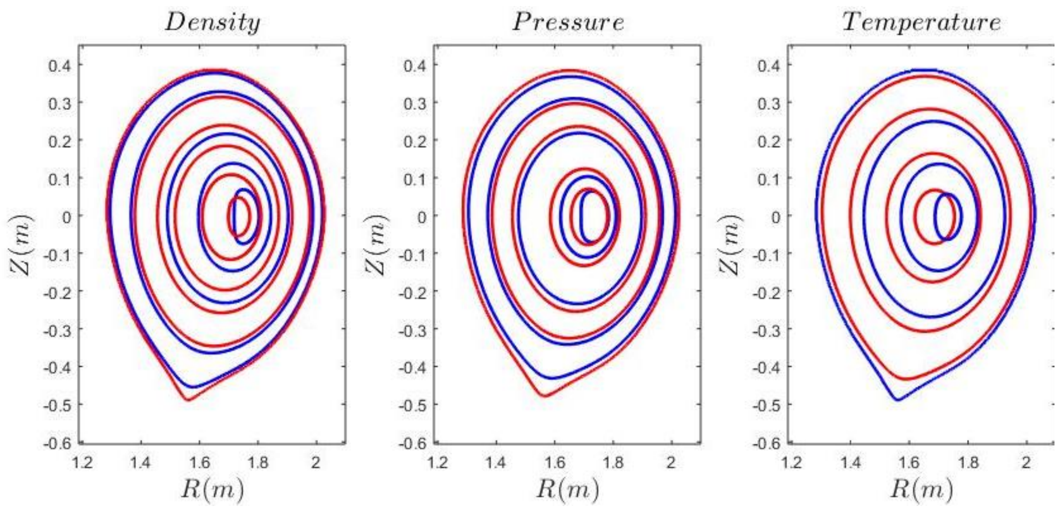

Figure 5. Density, pressure and Temperature contours for isentropic (blue) and isothermal (red) cases with a high toroidal flow.

VI. Conclusion and Discussion

In the paper, an extension of the CLT code to include a free-boundary equilibrium solver with a toroidal plasma flow and SOL, called CLT-EQ, was present. There are two kinds of construction schemes for the free boundary, namely 'divertor-type' and 'limiter-type'. Different regions, included the main plasma, SOL, the vacuum, and the 'private flux' region, are defined in the computational domain in order to design current sources. The Green's function method is adopted for external coils if these coils are located outside the computational domain. With toroidal plasma flow, the flux function is considerably different under the isentropic and isothermal assumptions. For the isentropic case, the entropy $S(\psi)$ is constant on magnetic surfaces. Four arbitrary functions $\theta_S(\psi)$, $S(\psi)$, $\Omega(\psi)$ and $F(\psi)$ are pre-required for an equilibrium. For the isothermal case, the plasma temperature $T(\psi)$ is a surface quantity due to large heat conductivity along magnetic field lines. Another four arbitrary functions $\theta_T(\psi)$, $T(\psi)$, $\Omega(\psi)$ and $F(\psi)$ are needed. The effects of the toroidal plasma flow on the Shafranov shift are investigated. In a high beta plasma, the magnetic shift due to the toroidal plasma flow are almost same for both the isentropic and isothermal cases and are about $0.04a_0$ at M_0=0.2. In addition, the X-point are slightly shifted upward by 0.0125 a_0. But in fact, the effect of the toroidal flow on the magnetic axis and the X-point shift may be neglected because M_0 is usually less than 0.05 in real tokamaks. The effects of the toroidal plasma flow on plasma parameters, such as the density, the pressure, and the temperature, are also investigated. The high toroidal flow shifts the plasma outward due to the centrifugal effect. But temperature profiles are noticeable difference in two cases because the plasma temperature is the flux function in the isothermal case.

Acknowledgments

This work was supported by the Chinese National Fusion Project for ITER under Grant Nos. 2019YFE03020003 and 2019YFE03030004, and the Nature Science Foundation of China (NSFC) under Grant Nos. 11775188 and 11835010.

Appendix

From the well-known thermodynamic relations

$$dh = dp/\rho + TdS$$

where h is the specific enthalpy. Considering the isentropic problem dS=0 and then $p = S\rho^\gamma$, $T = \rho^{\gamma-1}/(\gamma-1)$ [25][21], the following relation can be obtained:

$$h = \frac{\gamma}{\gamma - 1} S\rho^{\gamma-1}$$

where γ is the ratio of specific heat that is chosen to be 5/3 as usual. Considering the isentropic equilibrium with $\boldsymbol{v} \cdot \nabla S(\psi) = 0$, and multiplying the momentum equation by $\rho^{-1}\boldsymbol{B}$, the following expression is obtained by using $\boldsymbol{v} \cdot \nabla \boldsymbol{v} = -R\Omega^2(\psi)\nabla R$ and $\boldsymbol{B} \cdot \nabla \Omega = 0$

$$\begin{aligned} 0 &= \rho^{-1}\boldsymbol{B} \cdot \left(\rho \boldsymbol{v} \cdot \nabla \boldsymbol{v} + \nabla p - \mathbf{J} \times \mathbf{B}\right) \\ &= \boldsymbol{B} \cdot \left(\frac{\nabla p}{\rho} - \nabla R^2\Omega^2/2\right) \\ &= \boldsymbol{B} \cdot \nabla\left(h - R^2\Omega^2/2\right), \end{aligned}$$

which suggests that the Bernoulli equation is an arbitrary function of the poloidal flux, i.e.,

$$\theta_S(\psi) = h - R^2\Omega^2/2 = \frac{\gamma}{\gamma + 1} S\rho^{\gamma-1} - R^2\Omega^2/2$$

Now let us consider the isothermal equilibrium T(ψ). The plasma is assumed an ideal gas, $p(R,\psi) = T(\psi)\rho(R,\psi)$. Multiplying the momentum equation by $\rho^{-1}\boldsymbol{B}$, the following expression is obtained by using $\boldsymbol{v} \cdot \nabla \boldsymbol{v} = -R\Omega^2(\psi)\nabla R$ and $\mathbf{B} \cdot \nabla T = 0$

$$\begin{aligned} 0 &= \rho^{-1}\boldsymbol{B} \cdot \left(\rho \mathbf{v} \cdot \nabla \mathbf{v} + \nabla p - \mathbf{J} \times \mathbf{B}\right) \\ &= \boldsymbol{B} \cdot \left(-R\Omega^2 \nabla R + \nabla \rho T/\rho\right) \\ &= \boldsymbol{B} \cdot \left(-\nabla R^2\Omega^2/2 + T\nabla\rho/\rho\right) + R^2\Omega \boldsymbol{B} \cdot \nabla\Omega + \boldsymbol{B} \cdot \nabla T \\ &= \boldsymbol{B} \cdot \left(-\nabla R^2\Omega^2/2 + T\nabla \ln \rho + \ln \rho \nabla T\right) \\ &= \boldsymbol{B} \cdot \nabla\left(T \ln \rho - R^2\Omega^2/2\right), \end{aligned}$$

which indicates that $\theta_T(\psi) = T \ln \rho - R^2\Omega^2/2$ is also an arbitrary function of the poloidal flux. In order to ensure the flux surface quantity of $\theta_T(\psi)$, we need to carefully construct a density distribution function $\rho(R,\psi)$. With a referenced density distribution $\rho_0(\psi)$, we have

$$\theta_{T0}(\psi) = T \ln \rho_0(\psi) - \Omega^2 R_0^2/2$$

R_0 is the major radius. Thus, the density that is not a flux surface quantity can be expressed as follows,

$$\rho(\psi, R) = \rho_0(\psi) exp\left(\frac{\Omega^2 \left(R^2 - R_0^2\right)}{2T}\right)$$

And similarly, the pressure can also be expressed to be

$$p(\psi, R) = p_0(\psi) exp\left(\frac{\Omega^2 \left(R^2 - R_0^2\right)}{2T}\right)$$

Note that the relation $p_0(\psi) = T(\psi)\rho_0(\psi)$ must be satisfied. In other words, only two of the three parameters $p_0(\psi)$, $\rho_0(\psi)$ and $T(\psi)$ can be chosen freely. $\theta_T(\psi)$ constructed by this method can easily be proved to be the flux surface quantity,

$$\begin{aligned}
&\theta_T(\psi) = T \ln \rho(R,\psi) - R^2\Omega^2/2 \\
&= T \ln\left(\rho_0(\psi) exp\left(\frac{\Omega^2 \left(R^2 - R_0^2\right)}{2T}\right)\right) - R^2\Omega^2/2 \\
&= T ln \rho_0 - \Omega^2 R_0^2/2 \\
&= \theta_{T0}(\psi).
\end{aligned}$$

References

[1].J E Rice, A C Ince-Cushman, M L Reinke, Y Podpaly, M J Greenwald, B LaBombard and E S Marmar, “Spontaneous core toroidal rotation in Allocator C-Mod

L-mode, H-mode and ITB plasmas.," Plasma Physics and Controlled Fusion, 50(12):124042 (2008).

[2].Y. L. Wei, D. L. Yu, L. Liu, K. Ida, M. von Hellermann, J. Y. Cao, A. P. Sun, Q. Ma, W. J. Chen, Yi Liu, L. W. Yan, Q. W. Yang, X. R. Duan, and Yong Liu, "High spatial and temporal resolution charge exchange recombination spectroscopy on the HL-2A tokamak," Rev. Sci. Instrum. 85, 103503(2014).

[3].Yuejiang Shi, Guosheng Xu, Fudi Wang, Mao Wang, Jia Fu, Yingying Li, Wei Zhang, Wei Zhang, Jiafeng Chang, Bo Lv, Jinping Qian, Jiafang Shan, Fukun Liu, Siye Ding, Baonian Wan, Sang-Gon Lee, Manfred Bitter, and Kenneth Hill, "Observation of cocurrent toroidal rotation in the east tokamak with lower-hybrid current drive". Phys. Rev. Lett., 106:235001(2011).

[4].X. X. He, D. L. Yu, L. W. Yan, L. Liu, W. J. Chen, Y. L. Wei, X. F. He, Q. Ma, Z. B. Shi, Yi Liu, Q. W. Yang, M. Xu, and X. R. Duan, "Fast charge exchange recombination spectroscopy on huanliu-2a tokamak," Rev. Sci. Instrum. 91(5):053504(2020).

[5].M. Bitter, K. W. Hill, A. L. Roquemore, P. Beiersdorfer, S. M. Kahn, S. R. Elliott, and B. Fraenkel, "Imaging x-ray crystal spectrometers for the National Spherical Torus Experiment," Rev. Sci. Instrum. 70(1): 292–295(1999).

[6].John Howard, "High-speed high-resolution plasma spectroscopy using spatial-multiplex coherence imaging techniques(invited)," Rev. Sci. Instrum. 77(10): 10F111(2006).

[7].T. Long, J. S. Allcock, L. Nie, R. M. Sharples, M. Xu, R. Ke, S. Zhang, S. A. Silburn, J. Howard, Y. Yu, B. Yuan, Z. H. Wang, X. M. Song, L. Liu, and X. R. Duan, "Doppler coherence imaging of scrape-off-layer impurity flows in the HL-2A tokamak," Rev. Sci.

Instrum. 91(8): 083504(2020).

[8].S. Wang and Z. W. Ma, “Influence of toroidal rotation on resistive tearing modes in tokamaks,” Physics of Plasmas, 22(12):122504(2015).

[9].W. Zhang, Z.W. Ma, X.Q. Lu, and H.W. Zhang, “Influence of shear flows on dynamic evolutions of double tearing modes,” Nuclear Fusion, 60(12):126022(2020)

[10].A. Bondeson and D. J. Ward, “Stabilization of external modes in tokamaks by resistive walls and plasma rotation,” Phys. Rev. Lett. 72:2709–2712(1994).

[11].P.C. de Vries, M.-D. Hua, D.C. McDonald, C. Giroud, M. Janvier, M.F. Johnson, T. Tala, and K.-D. Zastrow and, “Scaling of rotation and momentum confinement in JET plasmas,” Nuclear Fusion, 48(6):065006(2008).

[12].Y. Koide, M. Kikuchi, M. Mori, S. Tsuji, S. Ishida, N. Asakura, Y. Kamada, T. Nishitani, Y. Kawano, T. Hatae, T. Fujita, T. Fukuda, A. Sakasai, T. Kondoh, R. Yoshino, and Y. Neyatani, “Internal transport barrier on q=3 surface and poloidal plasma spin up in JT-60U high-β_p discharges,” Phys. Rev. Lett. 72:3662–3665(1994).

[13].L. Li, Y.Q. Liu, Y. Liang, N. Wang, Q. Luan, F.C. Zhong and Y. Liu, “Screening of external magnetic perturbation fields due to sheared plasma flow,” Nucl. Fusion, 56,092008(2016)

[14].H W Zhang, X Lin, Z W Ma, W Zhang, and T E Bagwell, “Systematic simulation studies on the penetration of resonant magnetic perturbations in an Experimental Advanced Superconducting Tokamak,” Plasma Physics and Controlled Fusion, 63(3):035011(2021).

[15].H. Lütjens, A. Bondeson, and O. Sauter, “The CHEASE code for toroidal MHD equilibria,” Computer Physics Communications. 97(3): 219-260(1996)

[16].L. L. Lao, H. St. John, R. D. Stambaugh, A. G. Kellam, W. Pfeiffer, "Reconstruction of Current Profile Parameters and Plasma Shapes in Tokamaks, " Nucl. Fusion, 25, 1611 (1985)

[17].L. L. Lao, J. R. Ferron, R. J. Groebner, W. Howl, H. St. John, E. J. Strait and T. S. Taylor, "Equilibrium Analysis of Current Profiles in Tokamaks," Nucl. Fusion, 30, 1035(1990)

[18].Huysmanx, G. T. A. and Goedbloed, J.P. and Kerner, W, "Isoparametric Bicubic Hermite Elements for Solution of the Grad-Shafranov Equation," International Journal of Modern Physics C, 2(1):371-376(1991)

[19].J DeLucia and S.C Jardin and A.M.M Todd, "An iterative metric method for solving the inverse tokamak equilibrium problem," Journal of Computational Physics, 37(2):183-204(1980)

[20].L. Guazzotto, R. Betti, J. Manickam, and S. Kaye, "Numerical study of tokamak equilibria with arbitrary flow". Physics of Plasmas, 11(2):604–614(2004).

[21].Yanqiang Hu, Yemin Hu, and Nong Xiang, "Fixed boundary toroidal plasma equilibria with toroidal flows". Physics of Plasmas, 23(4):042506(2016).

[22].S. Semenzato, R. Gruber, and H. P. Zehrfeld, "Computation Of Symmetric Ideal MHD Flow Equilibria," Comput. Phys. Rep. 1:389-425 1984

[23].A.J.C.Beliën, M. Botchev, J. Goedbloed, B. van der Holst, and R. Keppens, "FINESSE: Axisymmetric MHD Equilibria with Flow," Journal of Computational Physics, 182:91-117(2002)

[24].R. F. Schmitt, L. Guazzotto, H. Strauss, G. Y. Park, and C.-S. Chang, "Free-boundary magnetohydrodynamic equilibria with flow," Physics of Plasmas,

18(2):022502(2011).

[25].E K Maschke and H Perrin, “Exact solutions of the stationary MHD equations for a rotating toroidal plasma,” Plasma Physics, 22(6):579–594(1980).

[26].Eliezer Hameiri, “The equilibrium and stability of rotating plasmas,” Physics of Fluids, 26(1):230–237(1983).

[27].Tatsuoki Takeda and Shinji Tokuda, “Computation of MHD equilibrium of tokamak plasma”. Journal of Computational Physics, 93(1):1–107(1991).

[28].W. J. Chen, D. L. Yu, L. W. Yan, B. S. Yuan, X. X. He, L. Liu, Y. L. Wei, N. Zhang, X. F. He, H. Wu, Z. B. Shi, Y. Liu, Q. W. Yang and the HL-2A Team, “Current profile reconstruction using motional stark effect polarimeter data on HL-2A tokamak,” Fusion Science and Technology, 76(1):37–44(2020).

[29].James D. Callen J. Leon Shohet William D. D’haeseleer, William N.G. Hitchon, “Flux Coordinates and Magnetic Field Struct,” Springer-Verlag Berlin Heidelberg, 1991.

[30].Ting WU, Min XU, Lin NIE, Yi YU, Jianqiang XU, Ting LONG, Yu HE, Jun CHENG, Longwen YAN, Zhihui HUANG, Rui KE, Peng SHI, Shuo WANG, and Bing LIU, “Effect of edge turbulent transport on scrape-off layer width on HL-2A tokamak,” Plasma Science and Technology, 23(2):025101(2021).

[31].ITER Physics Expert Group on Divertor, ITER Physics Expert Group on Divert Database, and ITER Physics Basis Editors. Chapter 4: Power and particle control. Nuclear Fusion, 39(12):2391–2469(1999).

[32].C S Pitcher and P C Stangeby, “Experimental divertor physics,” Plasma Physics and Controlled Fusion, 39(6):779–930(1997).

[33].H. L. STONE, “Iterative solution of implicit approximations of multidimensional partial differential equations,” SIAM J. Numer. Anal., 5:530–558(1968).

[34].G. F. PINDER, P. C. TRESCOTT and S. P. LARSON, “Finite-Difference Model for Aquifer Simulation in Two Dimensions with Results of Numerical Experiments,” Chap. C1, Book 7, Techniques of Water-Resources, Investigations of the United States Geological Survey, U.S. Geological Survey, Reston, Virginia, 1976.